

Quantum state reconstruction by high-frequency, time-domain, homodyne tomography

A. Zavatta

Istituto Nazionale di Ottica Applicata, L.go E.Fermi, 6, I-50125 Florence, Italy and Dept. of Systems and Computer Sciences, University of Florence, Florence, Italy

M. Bellini

Istituto Nazionale di Ottica Applicata, L.go E.Fermi, 6, I-50125 Florence, Italy

P.L. Ramazza

Istituto Nazionale di Ottica Applicata, L.go E.Fermi, 6, I-50125 Florence, Italy

F. Marin

Dept. of Physics, University of Florence, Florence, Italy

F.T. Arecchi

Istituto Nazionale di Ottica Applicata, L.go E.Fermi, 6, I-50125 Florence, Italy and Dept. of Physics, University of Florence, Florence, Italy

Abstract

We show a time-domain optical homodyne tomography achieved at very high frequencies for the reconstruction of quantum field states. A mode-locked Ti:Sa laser is used as the source for the local oscillator. The pulse trains are detected by two oppositely-biased silicon pin photodiodes and amplified by an high-bandwidth operational amplifier. This scheme is checked by means of standard techniques, including the Allan-variance analysis, and it is applied to the tomographic reconstruction of weak coherent states.

I. INTRODUCTION

Homodyne detection [1] has been extensively used to obtain tomographic reconstructions of CW optical fields, such as vacuum, coherent or squeezed states [2]. In order to access

states that exhibit stronger non-classical features, one has to exploit the higher nonlinearities made available by the high peak intensities of pulsed lasers. A frequency-domain approach, with a spectral analysis of the difference current in the homodyne photodetectors, was originally developed to study the noise in the field quadratures at definite radio-frequencies [3]. Successively, a pulsed balanced homodyne detection, consisting in the measurement of integrated photocurrents on single pulses, has been adopted to achieve a full reconstruction of weak field states [4,5]. The task of performing this time-domain homodyne detection is however quite demanding, since it requires very low electronic noise and high subtraction efficiencies over very large frequency bandwidths (from dc to a few times the repetition rate of the laser). Mostly due to these technical limitations, all the existing applications of the latter technique have been limited to pulse repetition rates well below the megahertz. Here we present an efficient pulsed optical homodyne apparatus that is able to work at the high repetition frequencies characteristic of the commonly used mode-locked laser systems. We have demonstrated its capabilities by tomographic reconstruction of weak coherent states with a mean photon number ($\langle n \rangle \sim 1$).

II. EXPERIMENTAL SETUP

The scheme of the experimental apparatus for homodyne measurements is shown in Fig. 1.

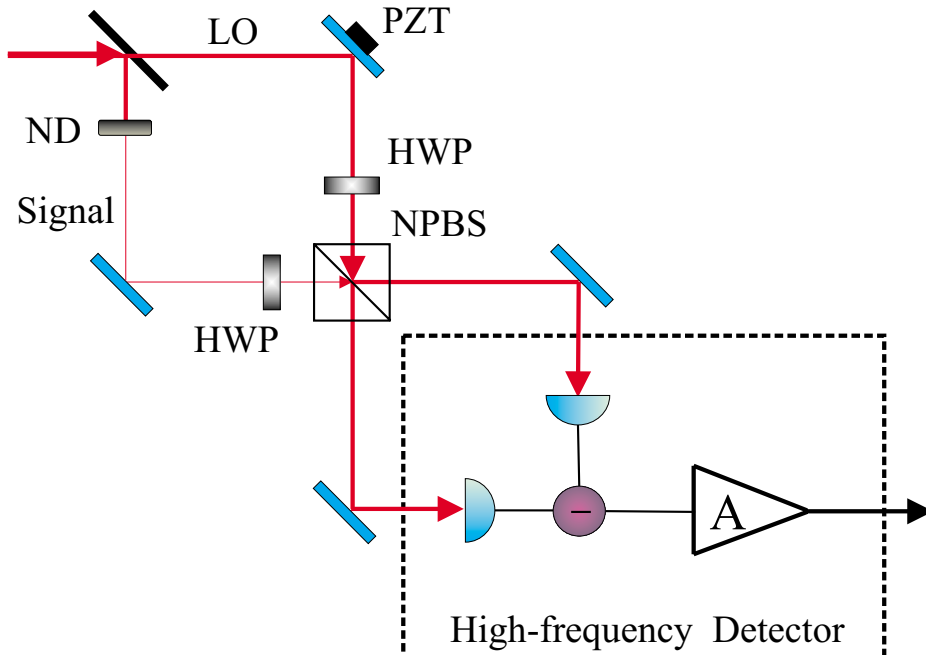


FIG. 1. Experimental setup: LO local oscillator beam; HWP half-wave plate; NPBS non-polarizing beam-splitter; A amplifier. PZT piezo-electric translation stage; ND neutral density filter.

A mode-locked Ti:sapphire laser (Spectra-Physics Tsunami), emitting trains of 3-ps pulses at 786 nm at a repetition rate of 82 MHz, is used as the source for the local oscillator (LO) beam. The total laser power can be varied by means of a half-wave plate

followed by a polarizer. A 50% cube beam-splitter mixes the LO with the field state under study and two 80-mm lenses focus the output beams onto the photodetectors. Since the beam-splitter is not perfectly insensitive to polarization, the balance between its two output ports is finely adjusted using half-wave plates.

For the measurement of the laser shot-noise, the signal port of the beam-splitter is blocked, so that only the vacuum field enters the apparatus.

The two pin photodiodes (PD) (EG&G FFD040) are connected together and oppositely biased. The signal generated on a load resistor is amplified with gain $G=10$ by an operational amplifier (Comlinear CLC 425) in a non-inverting configuration. The output signal is recorded by a spectrum analyzer or by a digital scope with a bandwidth of 1 GHz, a sampling rate of 4 GSamples/s and a storage depth of 200,000 points (LeCroy LC564). The overall detection efficiency η is measured by comparing the reading of a power meter with the mean photocurrent, obtaining a value of $\eta = 0.71 \pm 0.04$ for the two photodiodes.

III. FREQUENCY AND TIME-RESOLVED ANALYSIS OF THE VACUUM FLUCTUATIONS

By directing the laser pulse train on the PDs, we have checked that their frequency response curve is broad enough to isolate single pulses in the detected signal. The output pulses show a FWHM duration of about 5 ns and successive pulses, separated by 12 ns, result well distinct from each other.

Another key point of the apparatus is its ability to efficiently perform the difference between the amplitude fluctuations of the beams impinging on the two detectors. This is expressed by the Common Mode Rejection Ratio (CMRR) of the balanced detection, defined as the spectral power measured when both PDs are illuminated, divided by the power measured on one PD when the other one is blocked. We have measured it at the harmonic frequencies of the laser repetition rate, obtaining a CMRR of 42 dB, 15 dB and 20 dB respectively for the first second and third harmonic of the laser repetition rate. Higher harmonics exhibit lower CMRR due to the different response of the PDs at higher frequencies.

We have performed a more stringent test on the effective capability of the detection system to measure the quantum fluctuations of the signal, in spite of the non-ideal characteristics of the local oscillator and of the detectors. We have indeed checked that, when the input signal is the vacuum state, we can measure the shot-noise of the local oscillator. This is obtained by acquiring the noise spectrum for different values of the laser power impinging on the PDs.

The frequency integral of the power spectrum is plotted as a function of the detected power in Fig. 2, together with a second order polynomial fit. We have carried out the integration between 300 kHz and 150 MHz, excluding the peaks at the laser repetition rate. The constant term of the fitting function gives the electronic and thermal noise; the first-order term corresponds to the laser shot noise (reported in Fig. 2 with a dashed line); the second-order term is due to the residual laser excess noise after the balanced detection. The relevant signal in a homodyne detection is carried by the first-order term, while both the constant and the second-order terms give rise to unwanted excess Gaussian fluctuations.

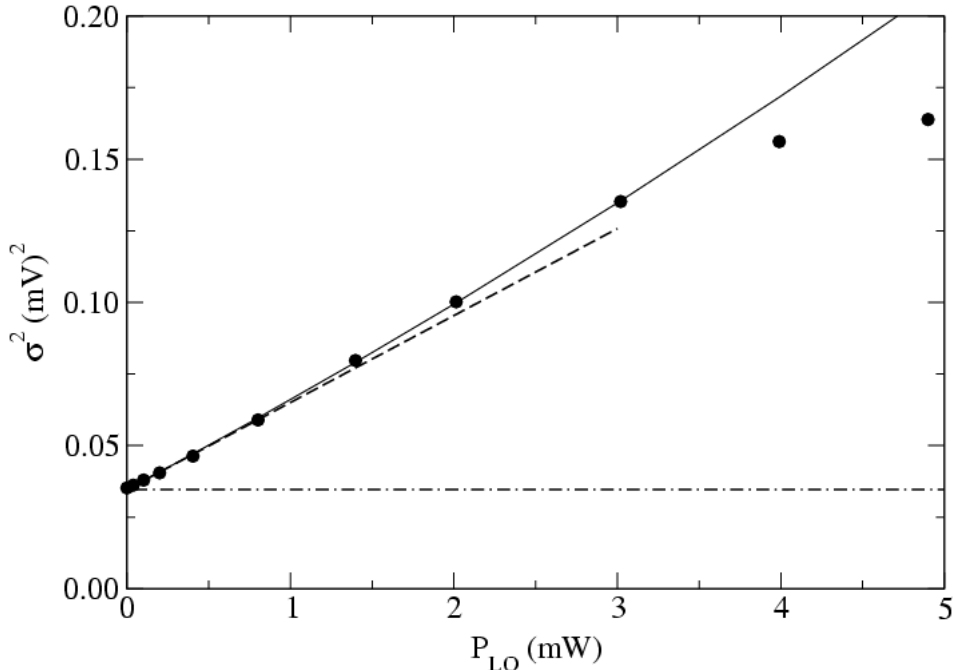


FIG. 2. Dots: integral of the power spectrum. Solid line: quadratic fit. Dashed line: shot-noise contribution. Dash-dotted line: electronic noise.

The optimum working power is around 3 mW, where about 70% of the fluctuations can be attributed to the first-order term.

The previous spectral analysis applies particularly well to a “quasi-cw” measurement system. Indeed the spectral properties are measured by the spectrum analyzer by means of a time integration over the sequence of laser pulses. Instead, our apparatus has the important additional property that the detection bandwidth allows pulse-selective experiments. It is therefore possible to evaluate properties of the pulsed light by considering the different pulses as separate events.

We report the experimental results obtained by means of three different analyzing techniques used for characterizing the pulsed, time resolved regime, namely, an off-line study of the variance of the pulse energy in time series, a more refined investigation on different time scales based on the Allan variance, and finally, the analysis of the fluctuations in laser pulses randomly acquired at a low rate.

For the off-line analysis, the output difference signal from the amplifier is stored in the digital scope. Time sequences of 200,000 samples, covering time windows of 50 μ s and including 4000 pulses each, are numerically integrated over time intervals of length $T = 12$ ns, corresponding to the separation between successive pulses, in order to extract the areas of all the pulses in the sequence and perform some statistics.

We have first evaluated the variance σ_{PE}^2 of the pulse energy over the recorded time series for different values of the laser average power, as shown in Fig. 3. This time-resolved

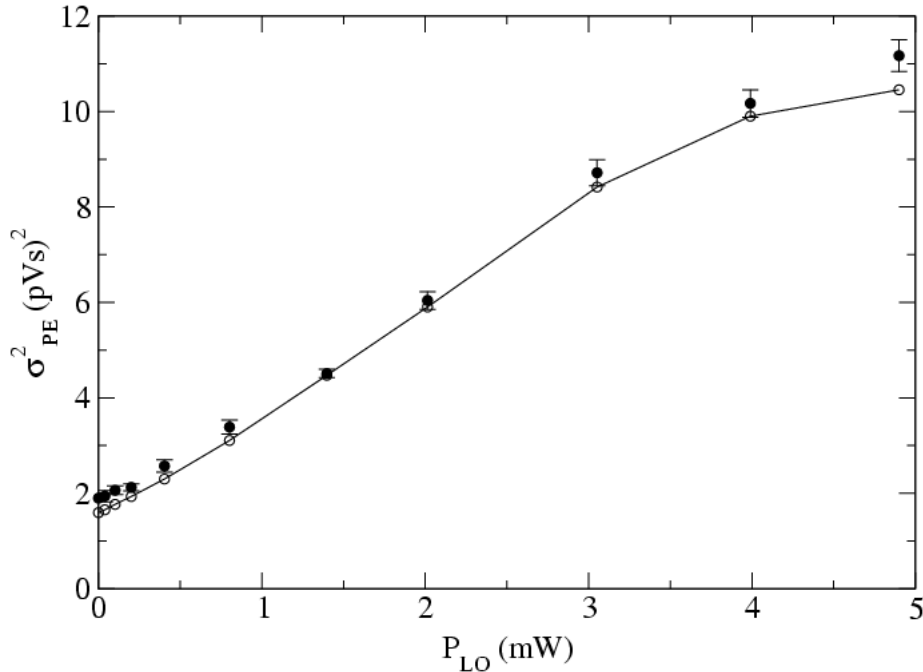


FIG. 3. Filled circles with error bars: directly measured σ_{PE}^2 ; empty circles: variance deduced from the spectrum according to (1).

analysis is directly related to the spectral analysis by

$$\sigma_{PE}^2 = 2T^2 \int_0^\infty S(\nu) \frac{\sin^2(\pi\nu T)}{(\pi\nu T)^2} d\nu. \quad (1)$$

The variance σ_{PE}^2 evaluated from the measured noise spectra according to eq.(1) is also reported in Fig. 3. It shows a very good agreement with the direct time-domain measurements, thus confirming the correctness of our approach.

Afterwards, we have performed a more refined time-resolved analysis on the pulse sequences stored in the scope. The study is based on the Allan variance σ_A^2 , defined as [6]

$$\sigma_A^2(\tau) = \frac{1}{2} \langle (f_{2,\tau} - f_{1,\tau})^2 \rangle, \quad (2)$$

where $f_{1,\tau}$ and $f_{2,\tau}$ are the integrals of the time-dependent signal $f(t)$ over two adjacent time intervals, both of duration τ . The brackets indicate the averaging over the whole time sequence.

In a time-resolved analysis, σ_A^2 has a role similar to the one played by the spectral density $S(\nu)$ in the spectral analysis. The spectral density $S(\nu)$ and the Allan variance are indeed related by the Cutler theorem

$$\sigma_A^2(\tau) = 4T^2 \int_0^\infty S(\nu) \frac{\sin^4(\pi\nu\tau)}{(\pi\nu\tau)^2} d\nu. \quad (3)$$

In the same way, the above evaluated variance σ_{PE}^2 corresponds to the weighted integral of the noise spectrum, as indicated by expression (1).

In our case of discretized time intervals, σ_A^2 is significant only when calculated over integer multiples $\tau = nT$ of the pulse separation T . Notice that in Fig. 4 we report a comparison

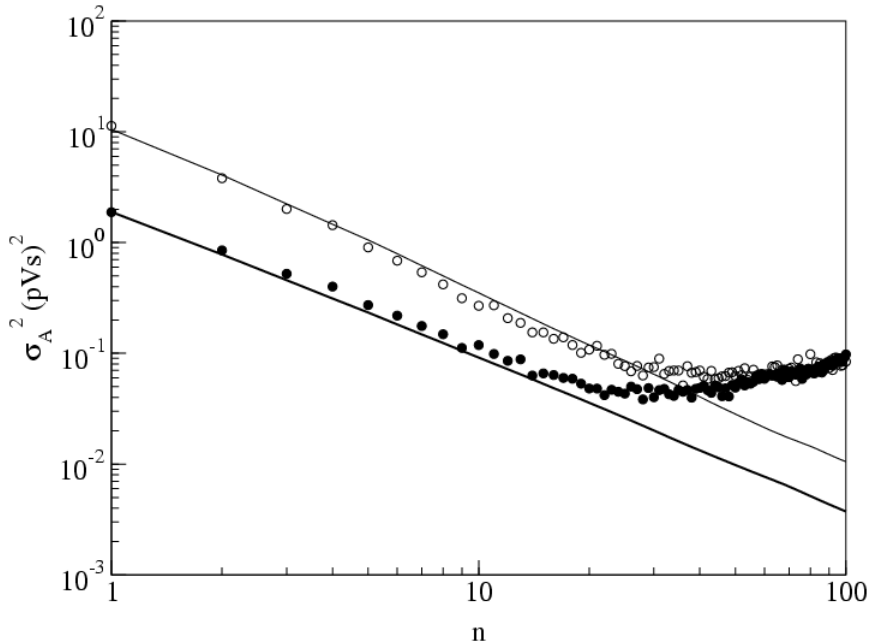


FIG. 4. Allan variance of the pulse energy. Empty symbols: with the laser power of 3 mW. Filled symbols: electronic noise. Solid lines: Allan variances calculated from the spectrum according to (4). The abscissa is in unit of T .

between the Allan variance measured in the time domain, and that obtained by integration of the noise spectral power using eq. (3).

The analysis of $\sigma_A^2(\tau)$ shows a τ^{-1} dependence for short τ , which corresponds to a white noise spectrum at high frequencies. As already discussed, in this spectrum there are contributions from electronic noise, shot noise and excess noise. For longer τ ($\gtrsim 20T$), we observe that the directly measured $\sigma_A^2(\tau)$ flattens due to $1/f$ noise. On the contrary, the variance deduced from the noise spectrum through eq. (3) does not deviate from the linear behavior observed for short τ .

This discrepancy is due to low frequency fluctuations in the digital scope electronics. A better pre-amplifier should allow for accurate measurements at least up to $\tau = 100T$.

IV. HOMODYNE TOMOGRAPHY

To perform a test of actual homodyne tomography with our high-frequency acquisition technique, we have slightly modified the experimental apparatus as shown in Fig. 1. A fraction of the laser power is splitted off the main (LO) beam and enters the second port of

the beam-splitter. We first achieve a good spatio-temporal overlap between this signal field and the LO by carefully adjusting the alignment mirrors and the path lengths (by means of two optical delay lines not shown in the figure) in the two arms of the so-formed Mach-Zender interferometer to obtain high-visibility interference fringes. Then the signal beam is strongly attenuated by means of calibrated neutral density filters and the beam path length in the LO arm is correspondingly compensated.

The relative phase between the two fields is controlled by applying a voltage to a piezoelectric transducer holding one of the mirrors in the LO beam path.

We have performed measurements of coherent states with different average photon numbers, ranging from 0 to about 5. Each measurement consists of 8 sequences of 4,000 pulses for each of the 25 values of the relative phase in the $[0, \pi]$ interval, for a total of 800,000 points per coherent state.

For each value of the relative phase θ between the LO field and the signal field, the histogram of the measured pulse energy difference represents the distribution $P_\theta(x)$ of the specific phase-rotated quadrature x . The collection of the distributions $P_\theta(x)$ for all θ allows the tomographic reconstruction of the quantum state of the radiation field. The tomographic reconstructing methods permit to obtain the Wigner function $W(x, y)$ in the quadrature phase-space [4] or the density matrix elements ρ_{nm} expressed in the Fock basis [7].

The reconstruction of the Wigner function is based on the fact that the distributions $P_\theta(x)$ are the marginal integrals of the Wigner function [8]

$$P_\theta(x) = \int_{-\infty}^{+\infty} W(x \cos \theta - y \sin \theta, x \sin \theta + y \cos \theta) dy. \quad (4)$$

Since the set of marginal distributions $\{P_\theta(x) : \theta \in [0, \pi]\}$ represent the Radon transform of the Wigner function, this one can be obtained by applying the inverse transformation to the measured $P_\theta(x)$. However, this method introduces an arbitrary cut-off parameter which should be carefully chosen in order to avoid the introduction of artifacts in the reconstructed function. In Fig. 5 we report the reconstructed Wigner functions in the case of the vacuum state (detected when the signal beam is blocked at the input of the homodyne beam splitter) and for a weak coherent field with a mean photon number $\langle n \rangle \sim 1$.

The second reconstruction procedure called ‘‘quantum sampling method’’ permits to reconstruct the density matrix elements without the introduction of any arbitrary parameter and also gives directly the estimation of the reconstruction errors. The probability distributions $P_\theta(x)$ are transformed according to

$$\rho_{nm} = \langle n | \hat{\rho} | m \rangle = \frac{1}{\pi} \int_0^\pi d\theta \int_{-\infty}^{+\infty} dx P_\theta(x) f_{nm}(x) e^{i(n-m)\theta}, \quad (5)$$

where f_{nm} are the factorized kernel functions called sampling functions [9]. The reconstructed diagonal elements of the density matrix ρ_{nn} are reported in Fig. 6 for three coherent states with different mean photon number. These values are well fitted by Poissonian distributions, as expected for coherent states.

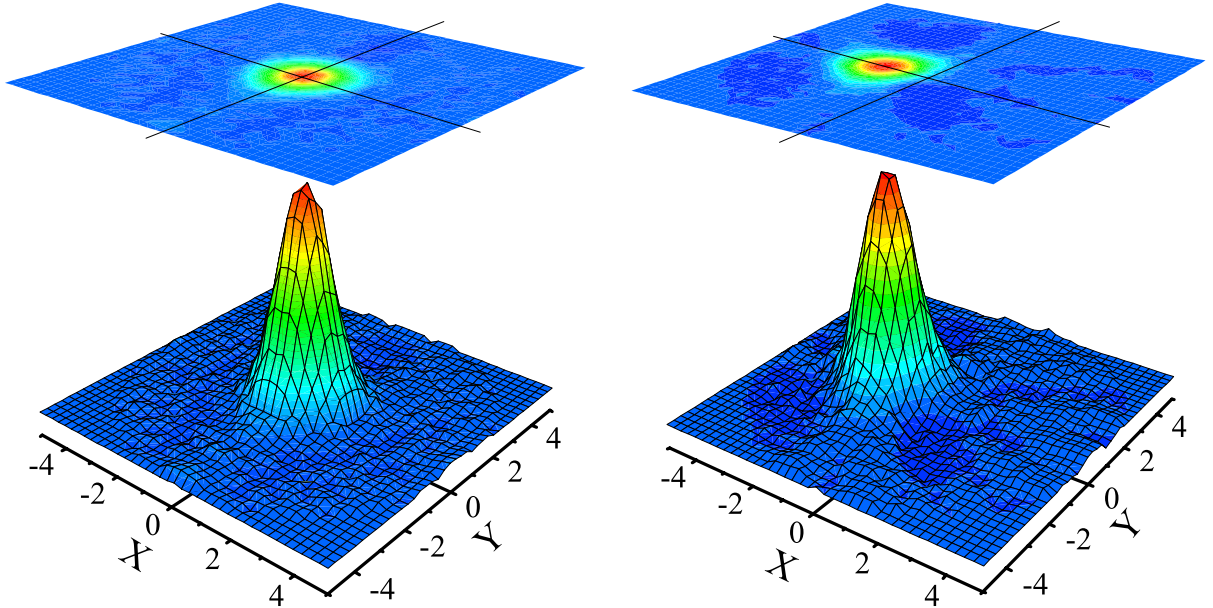


FIG. 5. Reconstructed Wigner functions: (a) vacuum state; (b) weak coherent state with $\langle n \rangle \sim 1$

V. CONCLUSIONS

We have presented a detection system suitable for homodyne measurements of quantum states generated by pulsed radiation at high repetition frequency. We have investigated the main features of a time resolved analysis of the homodyne signal, characterizing the system response both by means of standard indicators and of the Allan variance. This investigation allows to select the most useful time scale for better selecting quantum properties of the field. The results well compare with a standard spectral analysis.

With respect to the current setups, operating well below the megahertz, our approach allows an improvement of at least two orders of magnitude in the acquisition rate.

The demonstration of reliable quantum tomographic reconstruction at high frequencies opens new possibilities in the investigation of highly non-classical states of the electromagnetic field, such as mesoscopic Fock states generated by a low efficiency parametric generator or quantum superpositions of macroscopic states [10] (Schroedinger's cat-like states).

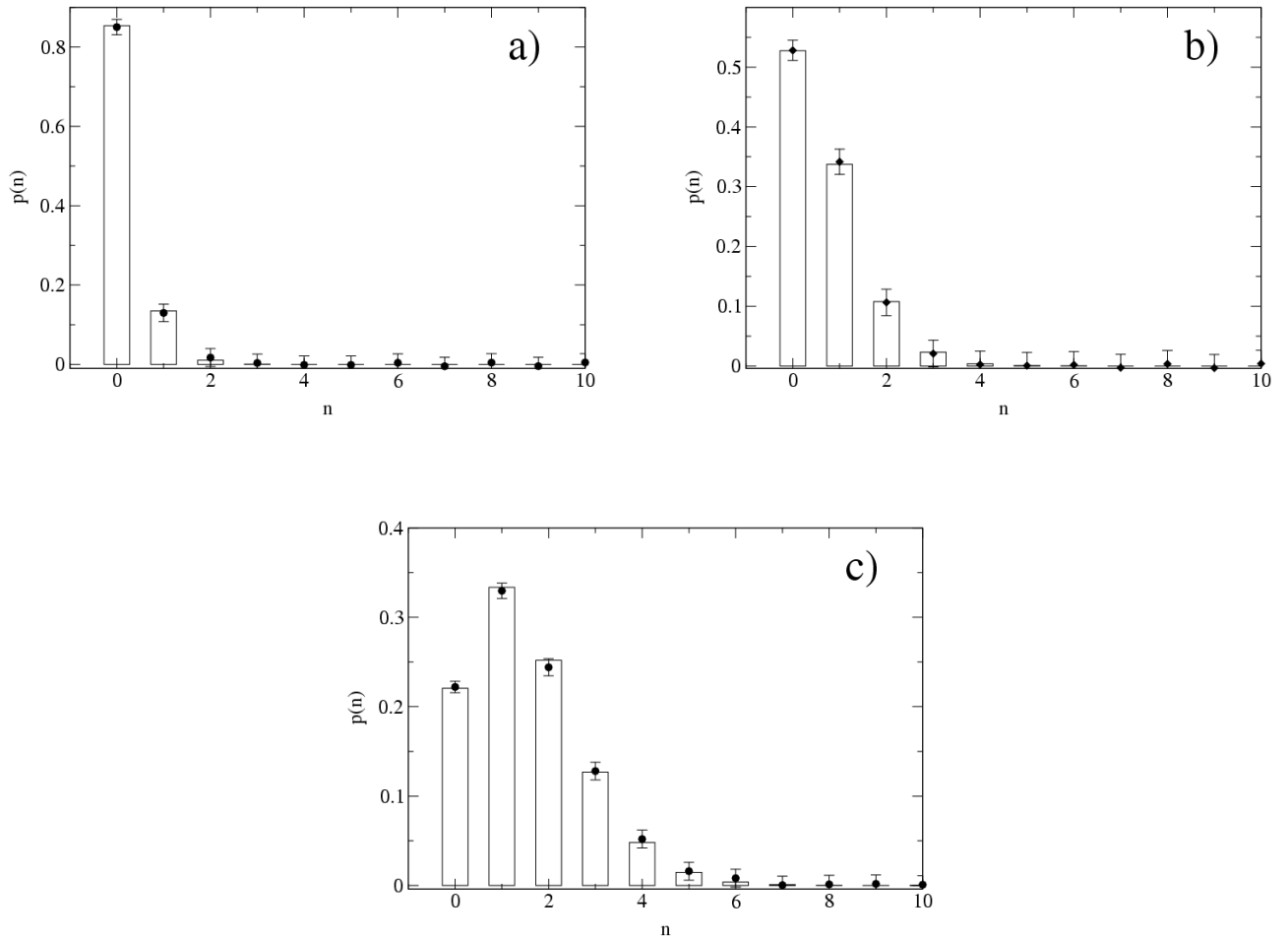


FIG. 6. Reconstruction of the photon statistics of three different coherent states. The points with error bars are the reconstructed values. The boxes are best fit Poissonian distribution values with: (a) $\langle n \rangle = 0.16$ photons/pulse; (b) $\langle n \rangle = 0.64$ photons/pulse and (c) $\langle n \rangle = 1.5$ photons/pulse.

REFERENCES

- [1] For a review see e.g. S. Reynaud, A. Heidmann, E. Giacobono and C. Fabre, “Quantum fluctuations in optical systems” in *Progress in Optics XXX*, E. Wolf ed. (Elsevier Science Publishers B.V.,1992). U. Leonhardt, *Measuring the quantum state of light* (Cambridge University Press, 1997).
- [2] G. Breitenbach, S. Schiller, and J. Mlynek, “Measurement of the quantum states of squeezed light,” *Nature* **387**, 471–475 (1997)
- [3] M. Vasilyev, S-K Choi, P. Kumar and G. M. D’Ariano, “Investigation of the photon statistics of parametric fluorescence in a traveling-wave parametric amplifier by means of self-homodyne tomography,” *Optics Lett.* **23**, 1393–1395 (1998)
- [4] D. Smithey, M. Beck, M.G. Raymer, and A. Faridani, “Measurement of the Wigner function distribution and the density matrix of a light mode using optical homodyne

- tomography: application to squeezed states and the vacuum,” *Phys. Rev. Lett.* **70** 1244–1247 (1993)
- [5] M. Crispino, G. Di Giuseppe, F. De Martini, P. Mataloni, and H. Kanatsoulis, “Towards a Fock-states tomographic reconstruction,” *Fortschr. Phys.* **48** 589–598 (2000)
- [6] D. W. Allan, “Statistics of Atomic Frequency Standard,” *Proc. IEEE* **54**, 221–230 (1966)
- [7] G.M. D’Ariano, C. Macchiavello, and M. G. A. Paris, “Detection of the density matrix through optical homodyne tomography without filtered back projection,” *Phys. Rev.* **50** 4298–4302 (1994)
- [8] K. Vogel, and H. Risken, “Determination of quasiprobability distribution in terms of probability distributions for rotated quadrature phase,” *Phys. Rev. A* **40**, 2847–2849 (1989)
- [9] U. Leonhardt, M. Munroe, T. Kiss, Th. Richter and M. G. Raymer, “Sampling of photon statistics and density matrix using homodyne detection,” *Optics Commun.* **127**, 144–160 (1996).
- [10] A. Montina, and F.T. Arecchi, “Toward an optical evidence of quantum interference between macroscopically different states,” *Phys. Rev. A* **58**, 3472–3476 (1998)